Applied Mathematics and Computation 324 (2018) 266–284

Contents lists available at ScienceDirect

Applied Mathematics and Computation

journal homepage: www.elsevier.com/locate/amc

Nonstandard finite differences for a truncated Bratu–Picard model

Paul Andries Zegeling, Sehar Iqbal*

Department of Mathematics, Utrecht University, The Netherlands

ARTICLE INFO

MSC:
34BXX
34B08
34B15
74G15
65NXX
65N06

Keywords:
Boundary value problems
Truncated Bratu–Picard model
Multiplicity
Existence
(Non)standard finite differences
Bifurcation diagram

ABSTRACT

In this paper, we consider theoretical and numerical properties of a nonlinear boundary-value problem which is strongly related to the well-known Gelfand–Bratu model with parameter λ. When approximating the nonlinear term in the model via a Taylor expansion, we are able to find new types of solutions and multiplicities, depending on the final index N in the expansion. The number of solutions may vary from 0, 1, 2 to ∞. In the latter case of infinitely many solutions, we find both periodic and semi-periodic solutions. Numerical experiments using a non-standard finite-difference (NSFD) approximation illustrate all these aspects. We also show the difference in accuracy for different denominator functions in NSFD when applied to this model. A full classification is given of all possible cases depending on the parameters N and λ.

1. Introduction

In this paper we consider smooth (continuous) solutions of the following truncated Bratu–Picard (tBP) model:

$$\begin{cases} u''(x) + \lambda \sum_{n=0}^{N} \frac{[u(x)]^n}{n!} = 0, \quad x \in [0,1], \quad \lambda \in \mathbb{R}, \quad N \in \mathbb{N} \cup \{0\} \cup \{\infty\}, \\ u(0) = u(1) = 0. \end{cases} \tag{1.1}$$

For $N = \infty$ and $\lambda \geq 0$, this yields the classical Gelfand–Bratu model [5,6,11,23] for which an exact solution is known, see among others [7] and Section 2.4. Traditionally, the names Bratu [5,6] and, sometimes, Gelfand [11] are coupled to this model. However, we propose to use the name Picard as well, since we found by performing a historical literature study that he was the first one who actually introduced the model, with non-unique solutions. His report on this model appeared two decades earlier than Bratu [5]. For more information on this observation, we would like to refer to the four-page note by Picard in [23].

The classical Gelfand–Bratu (GB) problem ($N = \infty$ and $\lambda \geq 0$) is a nonlinear elliptic (partial) differential equation, which finds, for example, its applications in combustion theory (the thermal ignition of a chemically active mixture of gasses) [4]. Other application areas of the GB problem appear in elasticity theory (membrane buckling) [26], in astronomy (gravitational equilibrium of polytropic stars and the Chandrasekhar model of the expansion of the universe) [8], in thermo-electro-hydrodynamic models and in nanotechnology (electrospinning processes) [28].

* Corresponding author.
E-mail address: s.iqbal@uu.nl (S. Iqbal).

https://doi.org/10.1016/j.amc.2017.12.005
0096-3003/

In previous numerical studies of the classical Gelfand–Bratu problem, several numerical methods have been proposed and compared to the exact solution. Most of these methods converge only to one of the two solutions of the model. Different computational techniques were compared with each other. For example, finite difference methods and multigrid methods are used in [21]. A direct shooting method and a Lie-group shooting method were presented in [1,7]. Further, perturbation iterations, parameter perturbations and parameter splines were implemented in [15]. Phase plane solutions for perturbation problems were given in [25]. Boyd's method [14] succeeded in giving both the lower and upper solutions, in case of multiple solutions. Buckmire [7] applied Mickens nonstandard finite difference method (NSFD) and compared the performances of the Adomian decomposition method, Boyd's pseudospectral method, nonlinear shooting method and standard finite difference (SFD) and NSFD methods. Buckmire reported that the NSFD method may converge to both solutions (the lower and the upper one) and is more accurate than SFD. A smart NSFD scheme for second order nonlinear boundary value problem has been discussed in Erdogan [10]. The related, more general, compact exponentially fitted method is used in [22] and SFD and NSFD approaches are considered as special cases. Recently an iterative finite difference method for solving the GB-model has been discussed in [13]. Mohsen [20] presented a straightforward solution technique of the 1D planar Bratu problem with different treatments of the resulting nonlinear system of equations by using SFD and NSFD methods. Mohsen recommended a simple sinusoidal function as an initial guess for NSFD which provides more accurate results.

Motivated by the recent articles of Mohsen [20] and Buckmire [7], we present a new and extended study of the tBP model of which the GB-model is a special case. We consider several cases of model (1.1) and investigate properties of the solution $u_\lambda^N(x)$ which depend on the parameter λ and the index N. We present several theoretical properties of the solution in which each solution of the model (1.1) has exactly one maximum and is symmetric at $x=\frac{1}{2}$ for $\lambda>0$. Previous articles considered only positive solutions but we consider all smooth solutions, where some of them are periodic and others are semi periodic. We also show theoretically and numerically that a unique solution exists for $\lambda\le 0$. We work out asymptotic expressions, to show the behavior of the solution for small and large values of the parameter λ. We present a further study of the NSFD scheme for iteratively solving the resulting nonlinear systems by choosing a simple sinusoidal function having the appropriate amplitude, as an initial guess. We observe that NSFD has a similar simplicity as an SFD approximation but it is slightly more accurate, in most cases. Numerical experiments show that a large number of solutions can be obtained which are either periodic or semi-periodic. In fact, the theory shows that infinitely many may exist. This is explored in an upcoming paper [30]. Graphically we also present the bifurcation nature of all possible cases of the tBP model (1.1). In literature, mainly positive solutions are considered for the $\lambda\ge 0$-case. In this paper, we give a full classification of all solution types of model (1.1), both positive or negative and (semi)-periodic, for all $\lambda\in\mathbb{R}$.

The paper is organized as follows. In Section 2, we present several theoretical, analytical and asymptotic properties of the solution and we also discuss exact solutions for some special cases of the truncated Bratu–Picard model (1.1). The SFD and NSFD approximations are worked out in Section 3. In Section 4, numerical experiments are performed to discuss the numerical aspects of the different cases of the truncated Bratu–Picard problem. All types of possible shapes of solutions (periodic and semi-periodic) and bifurcations are displayed in Section 5. In Section 6, we summarize the theoretical and numerical results.

2. Properties of the solution

We will denote solutions of the model (1.1) simply by $u(x)$ or, when it is appropriate, by $u_\lambda^N(x)$ to stress their dependence on the parameters λ and N.

2.1. General properties

We distinguish between several cases. For this, we define the following two subsets of $\mathbb{N}$:

$\mathcal{N}_2 := \{2,4,6,8,\ldots\}$,

$\mathcal{N}_3 := \{3,5,7,9,11,\ldots\}$.

Note, that the special cases $N=0$, $N=1$ and $N=\infty$ will be treated separately. Further, it is useful to define the functions

$$f(u)=f_N(u):=\sum_{n=0}^{N}\frac{u^n}{n!}\quad\text{and}\quad F(u):=\int_0^u f(\omega)\,d\omega.$$

In the following part, we describe and prove a series of analytical and asymptotic properties of the solution $u(x)$ of model (1.1).

Lemma 1. *For $N\in\mathcal{N}_2$, we have $f_N(u)>0$ for all $u\in\mathbb{R}$, whereas for $N\in\mathcal{N}_3$, $f_N(u)>0$ for all positive u and a unique value $\tilde{u}<0$ exists with $f_N(\tilde{u})=0$ (see also the four graphs in Fig. 1).*

Proof. Note that, for $u\ge 0$, automatically we find $f_N(u)>0$, since all single terms are positive and $f_N(0)=1$. Next, assume that $u<0$. Then $f_N'(u)=f_{N-1}(u)$ and $f_N(u)=f_{N-1}(u)+\frac{u^N}{N!}$. For $N\in\mathcal{N}_2$, we observe that $\lim_{u\to-\infty}f_N(u)=+\infty$. Suppose that there exists a value $\tilde{u}<0$ such that $f_N(\tilde{u})\le 0$. Then, there must be a $u^*<0$ such that $f_N(u^*)\le 0$ and $f_N'(u^*)=0$. At this

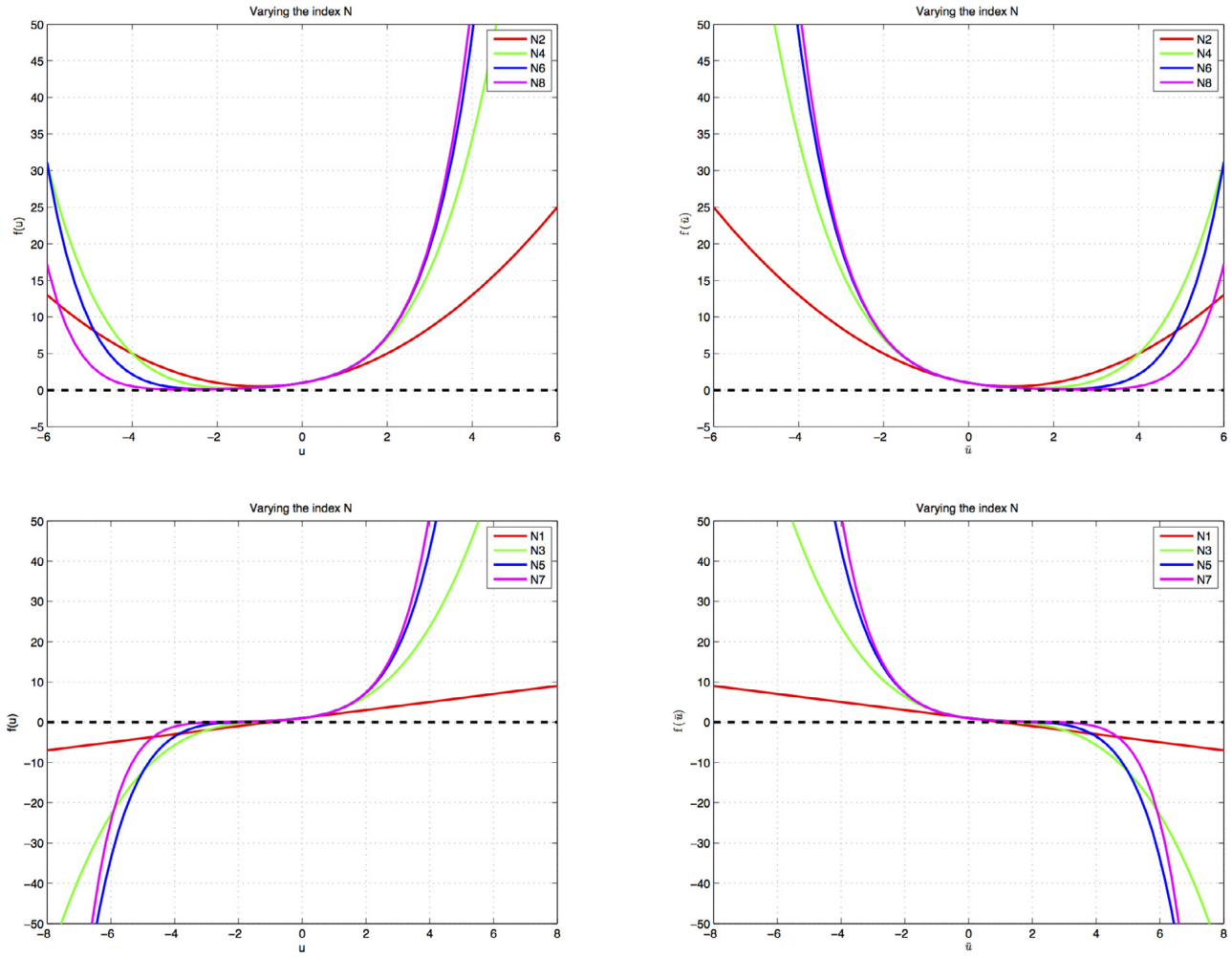

Fig. 1. The functions $f(u)$ and $f(\bar{u})$, for $N \in \mathcal{N}_2$ (upper two plots) are positive and for $N \in \mathcal{N}_3$ (lower two plots) they are both positive and negative.

minimum at $u = u^*$, we find:

$$f_N(u^*) = f'_N(u^*) + \frac{(u^*)^N}{N!} = \frac{(u^*)^N}{N!} > 0.$$

This contradiction shows that $f_N(u) > 0$ for $u < 0$. Therefore, $f(u) = f_N(u) > 0, \quad \forall u \in \mathbb{R}, \ N \in \mathcal{N}_2$. For the second part, suppose that $N \in \mathcal{N}_3$. Then $N-1$ is even and, as before, $f'_N(u) = f_{N-1}(u)$. Since $\lim_{u\to-\infty} f_N(u) = -\infty$, we conclude that there is a unique $\tilde{u} < 0$ such that $f_N(\tilde{u}) = 0$. □

Lemma 2. *For $N \in \mathcal{N}_2$, each solution $u(x)$ of model (1.1) is positive for $\lambda > 0$, and it is negative for $\lambda < 0$, respectively.*

Proof. From Lemma 1 and the fact that $\lim_{u\to 0} \frac{u}{\sum_{n=0}^{N} \frac{u^n}{n!}} = 0$ and $\lim_{u\to\infty} \frac{\sum_{n=0}^{N} \frac{u^n}{n!}}{u} = \infty$, we obtain the results in Section 3.1 in reference [2], that $u(x) \geq 0$ (for the case $\lambda > 0$). For the case $\lambda < 0$, we write $\bar{\lambda} := -\lambda > 0$ and $\bar{u} := -u$. Model (1.1) can then be written as:

$$\bar{u}'' + \bar{\lambda} \sum_{n=0}^{N} \frac{(-1)^n \bar{u}^n}{n!} = 0.$$

It is easily seen, using a similar proof as in Lemma 1 (cf. Fig. 1, upper plot on the right), that $f(\bar{u}) = \sum_{n=0}^{N} \frac{(-1)^n \bar{u}^n}{n!}$ is positive for $N \in \mathcal{N}_2$. Again, using Section 3.1 in [2], we conclude that $\bar{u}(x) \geq 0$, and, therefore, $u(x) = -\bar{u}(x) \leq 0$ for $\lambda \leq 0$. □

Lemma 3. *For $N \in \mathcal{N}_2 \cup \{\infty\}$, each solution $u(x)$ of model (1.1), if it exists, has exactly one maximum for $\lambda > 0$ and, in the case of $\lambda < 0$, one minimum.*

Proof. (We use elements from [3]): The trivial solution $u(x) \equiv 0$, $\forall x \in [0, 1]$ does not satisfy model (1.1), because $f(0) = 1$. This implies that $u(x)$ must have maximum (and/or minimum) values on the interval $x \in [0, 1]$. Assume, that this happens

at a point $x = x_0 \in [0, 1]$. Then $u'(x_0) = 0$ and also $u''(x_0) = -\lambda f(x_0)$. For $\lambda > 0$, we find $u''(x_0) < 0$, since $f(x_0) > 0$. Thus, we have a maximum at $x = x_0$. As $u''(x) < 0$ for all $x \in [0, 1]$, there is no minimum and there can not occur further maxima: the unique maximum is found at $x = x_0$. In the case $\lambda < 0$, a similar proof, using the fact that then $u'' > 0$, shows the existence of a unique minimum at $x = x_0$. □

Lemma 4. *For $N \in \mathcal{N}_2 \cup \{\infty\}$, each solution $u(x)$ of model (1.1) attains its* maximum *value at $x = \frac{1}{2}$ for $\lambda > 0$ (and its minimum value for negative λ). For $\lambda \in \mathbb{R}$, the solution is symmetric around $x = \frac{1}{2}$ in the following sense: $u(x) = u(1 - x)$.*

Proof. (we follow a proof similar to the one in [16]): First, we treat the case $\lambda > 0$. From Lemma 3 a unique maximum is obtained at $x = x_0$, i.e. $||u||_\infty = u(x_0)$. It is obvious that $u'(x) \geq 0$ on $[0, x_0]$ and $u'(x) \leq 0$ on $[x_0, 1]$. Integrating Eq. (1.1), we obtain:

$$\frac{1}{2}[u'(x)]^2 + \lambda F(u(x)) = \lambda F(||u||_\infty),$$

where we have used the constraints $F(u(x_0)) = F(||u||_\infty)$ and $u'(x_0) = 0$. Integrating once more, we find:

$$\sqrt{2\lambda}\; x = \int_0^u \frac{d\omega}{\sqrt{F(||u||_\infty) - F(\omega)}}, \quad \text{for } 0 \leq x \leq x_0,$$

and

$$\sqrt{2\lambda}\; (1 - x) = \int_0^u \frac{d\omega}{\sqrt{F(||u||_\infty) - F(\omega)}}, \quad \text{for } x_0 \leq x \leq 1.$$

Setting $x = x_0$ and $u(x_0) = ||u||_\infty$, it follows that x_0 must be the point $\frac{1}{2}$ and that $u(x) = u(1 - x)$, i.e., any solution of (1.1) is symmetric around the point $x = \frac{1}{2}$. The case $\lambda < 0$ is treated similarly, with the maximum replaced by the minimum. □

Lemma 5. *The solution $u(x)$ of model (1.1) is unique for $\lambda \leq 0$ and for any value of $N \in \mathbb{N}$.*

Proof. (This is a modified version of the proof in [12]): Suppose that there exist two solutions: $u_1(x)$ and $u_2(x)$ with $u_1'(0) \neq u_2'(0)$. It is no restriction to set $u_1'(0) > u_2'(0)$. Using the continuity of the solutions, we have $u_1'(x) > u_2'(x)$ on some interval $x \in [0, x_1]$. Suppose that at $x = x_1$: $u_1'(x_1) = u_2'(x_1)$. At this point, we have

$$u_1''(x_1) = \lim_{h \downarrow 0} \frac{u_1'(x_1) - u_1'(x - h)}{h} \text{ and } u_2''(x_1) = \lim_{h \downarrow 0} \frac{u_2'(x_1) - u_2'(x_1 - h)}{h}.$$

Then:

$$u_2''(x_1) - u_1''(x_1) = \lim_{h \downarrow 0} \frac{u_1'(x_1 - h) - u_2'(x_1 - h)}{h} \geq 0,$$

since $h > 0$ and $u_1'(x) > u_2'(x)$ on $[x_1 - h, x_1]$. From this follows: $u_2''(x_1) \geq u_1''(x_1)$. Next, write:

$$u_1(x) = \int_0^x u_1'(\omega) d\omega \quad \text{and} \quad u_2(x) = \int_0^x u_2'(\omega) d\omega.$$

This yields: $u_2(x_1) = \int_0^{x_1} u_2'(\omega) d\omega < \int_0^{x_1} u_1'(\omega) d\omega = u_1(x_1)$. Note that $f'(u) > 0$, which gives $f(u_1(x_1)) > f(u_2(x_1))$, as $u_1(x_1) > u_2(x_1)$. This makes a contradiction, because

$$u_2''(x_1) = f(u_2(x_1)) < f(u_1(x_1)) = u_1''(x_1).$$

Conclusion: there is only one solution. □

Lemma 6. *For $0 < \lambda \ll 1$, we find for any value of $N \in \mathbb{N}$ the following asymptotic expressions for the solution with the lowest maximum: $u(x) = \frac{\lambda}{2} x(1 - x) + \frac{1}{24} x(1 - 2x^2 + x^3)\; \lambda^2 + \mathcal{O}(\lambda^3)$ and $||u||_\infty = \frac{\lambda}{8} + \frac{5}{384}\lambda^2 + \mathcal{O}(\lambda^3)$.*

Proof. Assume that the solution can be written as an asymptotic series in the (small) parameter λ:

$$u(x) = u_0(x) + \lambda u_1(x) + \lambda^2 u_2(x) + \ldots$$

Substituting this series in Eq. (1.1) and collecting the different terms for the powers of λ, we find:

$$\begin{cases} \text{for } \lambda^0: \; u_0(x) = 0, \\ \text{for } \lambda^1: \; u_1(x) = \frac{1}{2} x(1 - x), \\ \text{for } \lambda^2: \; u_2(x) = \frac{1}{24} x(1 - 2x^2 + x^3), \\ \ldots \end{cases} \tag{2.1}$$

The results follow from Eq. (2.1) and by taking the maximum norm (see also the book by Verhulst [27] for more details). □

Lemma 7. *For $0 < \lambda \ll 1$ and $N = 2$, two solutions exist of which the lower solution is $u(x) = \mathcal{O}(\lambda)$ and the upper solution is $u(x) = \mathcal{O}(\frac{1}{\lambda})$.*

Proof. Write $u(x) = \lambda^\beta v(x)$ with $v(x) = \mathcal{O}(1)$ and $\beta \in \mathbb{R}$ to be determined (note that, in such a way, we cover all possible scales in u). Substituting this into model (1.1) with $N = 2$, we obtain

$$\lambda^\beta v'' + \lambda + \lambda^{\beta+1} v + \frac{1}{2}\lambda^{2\beta+1} v^2 = 0.$$

Significant degenerations (see Eckhaus [9], Verhulst [27]) appear only for the values $\beta = 1$ and $\beta = -1$. The case $\beta = 1$ is exactly the solution already obtained in Lemma 6, which is $\mathcal{O}(\lambda)$ and characterizes the 'lower' solution of the two. For the case $\beta = -1$, we find

$$v'' + \lambda^2 + \lambda v + \frac{1}{2} v^2 = 0.$$

Substituting the asymptotic series $v = v_0 + \lambda v_1 + \lambda^2 v_2 + \ldots$ and collecting terms of equal order, we find, for λ^0:

$$v_0'' + \frac{1}{2} v_0^2 = 0, \;\; v_0(0) = v_0(1) = 0.$$

From this differential equation, one could extract v_0 (a unique solution v_0 exists, see [24], p. 241, case 2), and similarly for the λ^1 terms, v_1, etcetera. Indeed, this then would give the asymptotic solution:

$$u(x) = \frac{1}{\lambda} v_0(x) + v_1(x) + \lambda v_2(x) + \cdots = \mathcal{O}(\frac{1}{\lambda}).$$

This is the second ('upper') solution. No other degenerations (values of β, or scales) can be found, so that one can conclude that two solutions exist for $\lambda \ll 1$. □

The results might be extended to other values of N. However, for $N > 2$, the number of significant degenerations increases significantly. It is not obvious which of those degenerations should be used, in general.

Lemma 8. *For $\lambda \gg 1$ and $N = 2$, no strictly positive solution exists for model (1.1).*

Proof. Define $\varepsilon := \frac{1}{\lambda} \ll 1$. Then model (1.1) can be rewritten as:

$$\varepsilon u'' + 1 + u + \frac{1}{2} u^2 = 0, \;\; u(0) = u(1) = 0, \;\; 0 < \varepsilon \ll 1.$$

We now write the asymptotic series as $u = u_0 + \varepsilon u_1 + \varepsilon^2 u_2^2 + \cdots$. The terms for ϵ^0 give: $1 + u_0 + \frac{1}{2} u_0^2 = 0$ which has no solution, since $1 + u_0 + \frac{1}{2} u_0^2$ is always positive. Therefore, we can not find u_0, and neither the functions u_1, u_2, ..., since they can only follow from (the non-existent) u_0. To cover all scales, we introduce $u(x) = \varepsilon^\gamma w(x)$ with $w(x) = \mathcal{O}(1)$ and $\gamma \in \mathbb{R}$. The only significant degenerations are $\gamma = 1$ and $\gamma = -1$ (see [9]). However, when calculating the first order term, these two values of γ yield contradictions as well. The conclusion is that for $\lambda \gg 1$ no solutions exist. □

Conjecture 9. *For $\lambda > 0$ and for $N \in \mathcal{N}_3$, infinitely many solutions $u(x)$ for model (1.1) exist. All solutions are either periodic or semi-periodic. We give numerical evidence in Section 4 to support this conjecture. A theoretical proof can be found in [30].*

2.2. Exact solutions for $N = 0$

For $N = 0$, Eq. (1.1) reduces to:

$$u''(x) + \lambda = 0, \tag{2.2}$$

and we can directly solve it. The solution reads:

$$u_\lambda^0(x) = \frac{\lambda}{2} x(1 - x) \tag{2.3}$$

with a maximum value of $||u_\lambda^0||_\infty = \frac{|\lambda|}{8}$. In the phase plane (u, u') no critical points are present (see Fig. 2).

2.3. Exact solutions for $N = 1$

For $N = 1$, model (1.1) is linear:

$$u''(x) + \lambda(1 + u(x)) = 0. \tag{2.4}$$

We have to distinguish between three different subcases. For $\lambda < 0$, the solution has the form:

$$u(x) = u_\lambda^1(x) = -1 + \frac{1}{e^{\sqrt{-\lambda}} - e^{-\sqrt{-\lambda}}} [(1 - e^{-\sqrt{-\lambda}}) e^{\sqrt{-\lambda} x} + (e^{\sqrt{-\lambda}} - 1) e^{-\sqrt{-\lambda} x}]. \tag{2.5}$$

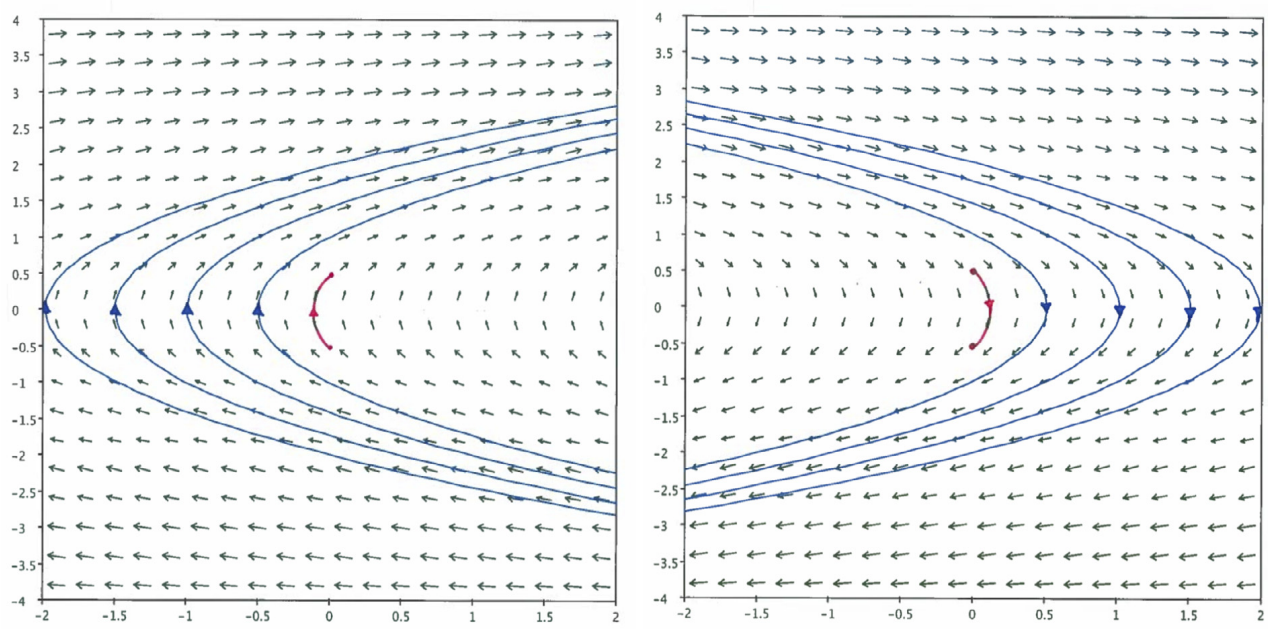

Fig. 2. The phase plane (u, u') for $N = 0$ with $\lambda < 0$ (left) and $\lambda > 0$ (right): no critical points are present. The red curves represent solutions satisfying the two boundary conditions.

Note that for $\lambda \to -\infty$ there is a horizontal asymptote: $||u_\lambda^1||_\infty \uparrow 1$. For $\lambda = 0$, we find the trivial solution $u_\lambda(x) \equiv 0$, and, for $\lambda > 0$, $\lambda \neq (m\pi)^2$, we obtain:

$$u(x) = u_\lambda^1(x) = -1 + \cos(\sqrt{\lambda}x) + \frac{1 - \cos(\sqrt{\lambda})}{\sin(\sqrt{\lambda})} \sin(\sqrt{\lambda}x). \tag{2.6}$$

For $\lambda = (m\pi)^2$ $(m \in \{2, 4, 6, \ldots\})$, there exist infinitely many solutions satisfying the differential equation and the two boundary conditions: $u_\lambda^1(x) = \sin(m\pi x)$, whereas for $\lambda = (m\pi)^2$ $(m \in \{3, 5, 7, \ldots\})$ no continuous solutions exist. These solutions seem to have singularities. Only for $\lambda \to (m\pi)^2$ with $m \in \{1, 3, 5, \ldots\}$ we find $||u_\lambda^1||_\infty \to \infty$. For the other values of m, i.e. $m \in \{2, 4, 6, \ldots\}$, there is no singularity at $\lambda = (m\pi)^2$, which can be checked easily using a Taylor series. The behaviour of $||u_\lambda^1||_\infty$ as a function of λ can be found in Section 5. In the phase-plane (u, u'), the model possesses a critical point to the left of the solution trajectory: a saddle point in the left half plane for $\lambda < 0$, whereas it has a center point for positive λ-values (see Fig. 3).

2.4. Exact solutions for $N = \infty$

For $N = \infty$, the second term in (1.1) becomes the Taylor series of the exponential function $e^{u(x)}$ around zero. We then arrive at the 'standard' Gelfand–Bratu model:

$$\begin{cases} u''(x) + \lambda e^{u(x)} = 0, & x \in [0, 1], \quad \lambda \in \mathbb{R}, \\ u(0) = u(1) = 0. \end{cases} \tag{2.7}$$

For positive λ (see, for instance, Buckmire [7]), the exact solution is characterized by the following expression:

$$\begin{cases} u(x) = u_\lambda^\infty(x) = -2 \ \ln \left[\dfrac{\cosh\left(\left(x - \frac{1}{2}\right)\frac{\theta}{2}\right)}{\cosh\left(\frac{\theta}{4}\right)} \right], \\ \theta = \sqrt{2\lambda} \cosh\left(\dfrac{\theta}{4}\right). \end{cases} \tag{2.8}$$

It is well known that for $0 < \lambda < \lambda_c$ there exist exactly two solutions to model (2.7), precisely one solution for $\lambda = \lambda_c$ and no solutions exist for $\lambda > \lambda_c$. Fig. 4 illustrates the possible solutions. The value for $\lambda_c = 3.513830719\ldots$ can be found numerically using the second formula in Eq. (2.8) and applying a Newton–Raphson method as described in [7]. In literature, only solutions for positive λ are given. Here, we would like to consider the case $\lambda < 0$ as well. It can be checked that the solution

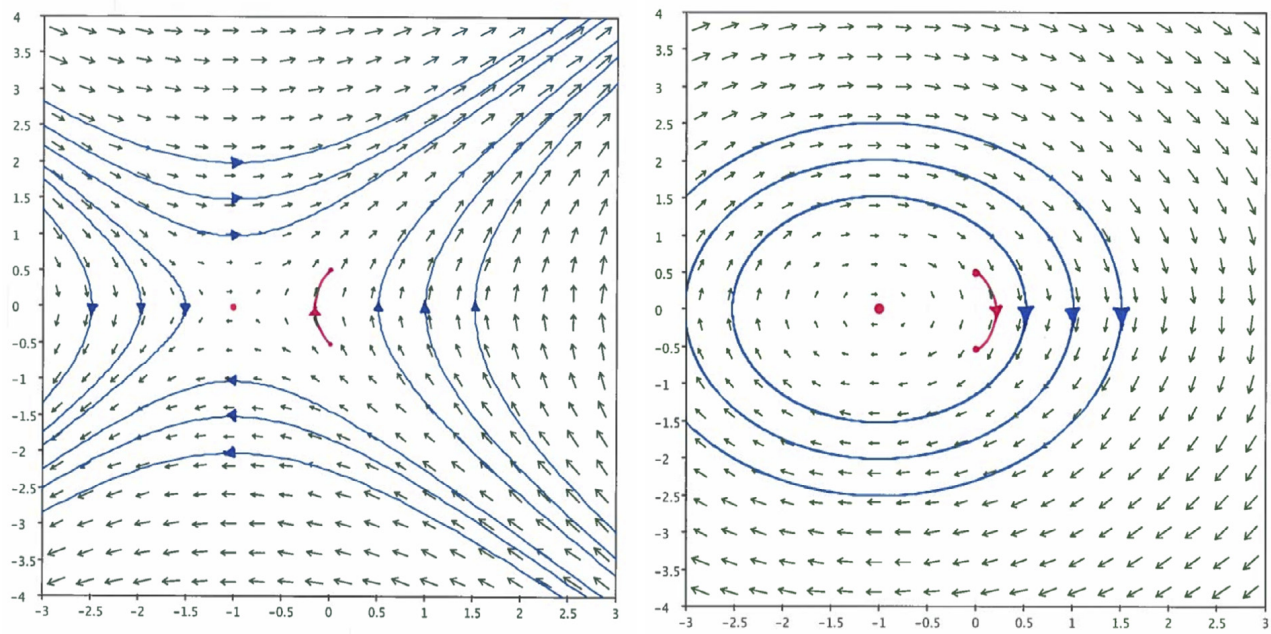

Fig. 3. The phase plane (u, u') for $N = 1$ for $\lambda < 0$ (left) and $\lambda > 0$ (right): a saddle point (left) and a center point (right) appear in this case, as indicated by the red bullets. The red curves represent solutions satisfying the two boundary conditions. (For interpretation of the references to color in this figure legend, the reader is referred to the web version of this article.)

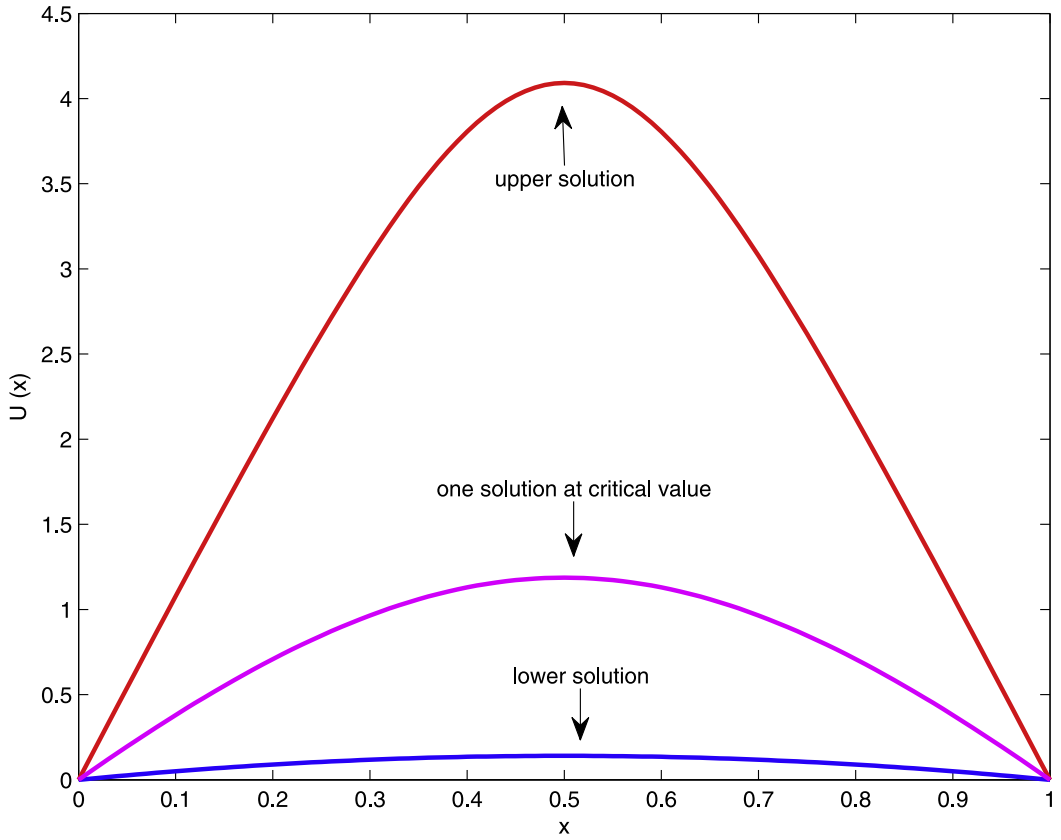

Fig. 4. The solutions for $N = \infty$ depending on the values of λ.

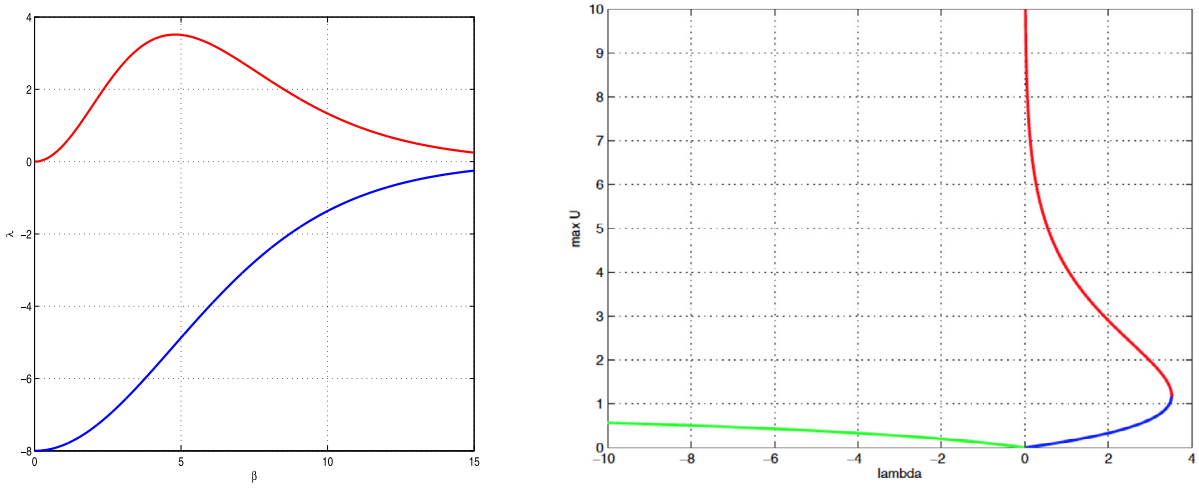

Fig. 5. In the left frame, we display the difference between unique solutions for negative λ (blue curve) and the three possible cases for positive λ (red curve) depending on the parameter β as explained in the text. In the right frame a bifurcation diagram for $N = \infty$ is given. Here, the blue and red lines indicate the two solutions for each positive $\lambda < \lambda_c \approx 3.514$ and the green line depicts the unique solution for all negative λ, respectively. (For interpretation of the references to color in this figure legend, the reader is referred to the web version of this article.)

then is given by:

$$\begin{cases} u(x) = u_\lambda^\infty(x) = -2\ \ln\left[\dfrac{\cos\left(\left(x-\frac{1}{2}\right)\frac{\theta}{2}\right)}{\cos\left(\frac{\theta}{4}\right)}\right], \\ \theta = \sqrt{-2\lambda}\cos\left(\dfrac{\theta}{4}\right). \end{cases} \tag{2.9}$$

For deriving this expression, one can use the relation $\cosh(ix) = \cos(x)$, among others. Furthermore, Lemma 5 states that a unique (smooth) solution $u_\lambda^\infty(x)$ exists for this case. Fig. 5 (left panel) gives an overview of the differences between positive and negative values of λ. The parameter β on the horizontal axis is connected to one of the two integration constants, after formally integrating equation (2.7). Note that on the vertical axis (in the right panel) we display the absolute maximum value of the solution as a function of the parameter λ. In this figure the specific cases, as already discussed above, can be detected easily. Note that still additional *singular* solutions may occur for $\lambda < 0$. For example we have, for $\lambda = -\pi^2$ (see [29]):

$$u_\lambda^\infty(x) = -\ln\left(1+\cos\left[\left(\frac{1}{2}+x\right)\pi\right]\right),$$

which blows up at $x = \frac{1}{2}$. In Fig. 5 (right panel) another way of representing the different cases as a function of λ is displayed: The green curve shows the unique solution for $\lambda < 0$. The blue and red curves illustrate the two positive solutions lower and upper respectively for $0 \le \lambda \le \lambda_c$ and no solution for $\lambda > \lambda_c$.

2.5. The case: $N \in \mathcal{N}_2$

As a characteristic example we take $N = 2$:

$$u''(x) + \lambda\left(1 + u(x) + \frac{1}{2}u(x)^2\right) = 0. \tag{2.10}$$

This case and all other values in $\mathcal{N}_2$ are topologically equivalent with the $N = \infty$ case, in the sense that there exist two, one or zero solutions u_λ^N, for positive λ, with a critical value $\lambda_c^N \approx 3.96$ for $N = 2$ (its precise value in general depends, of course, on N). We obtained the bifurcation curve when we consider the positive solutions, which resembles with the similar behavior of classical GB model. For negative λ values there is a unique solution (see Lemma 5). As mentioned, similar conclusions can be made for the cases $N = 4, 6, 8, \ldots$. Numerical solutions are given in Section 4.2.

2.6. The case: $N \in \mathcal{N}_3$

As characteristic examples we take $N = 3$ and $N = 5$:

$$u''(x) + \lambda\left(1 + u(x) + \frac{1}{2}u(x)^2 + \frac{1}{6}u(x)^3\right) = 0, \tag{2.11}$$

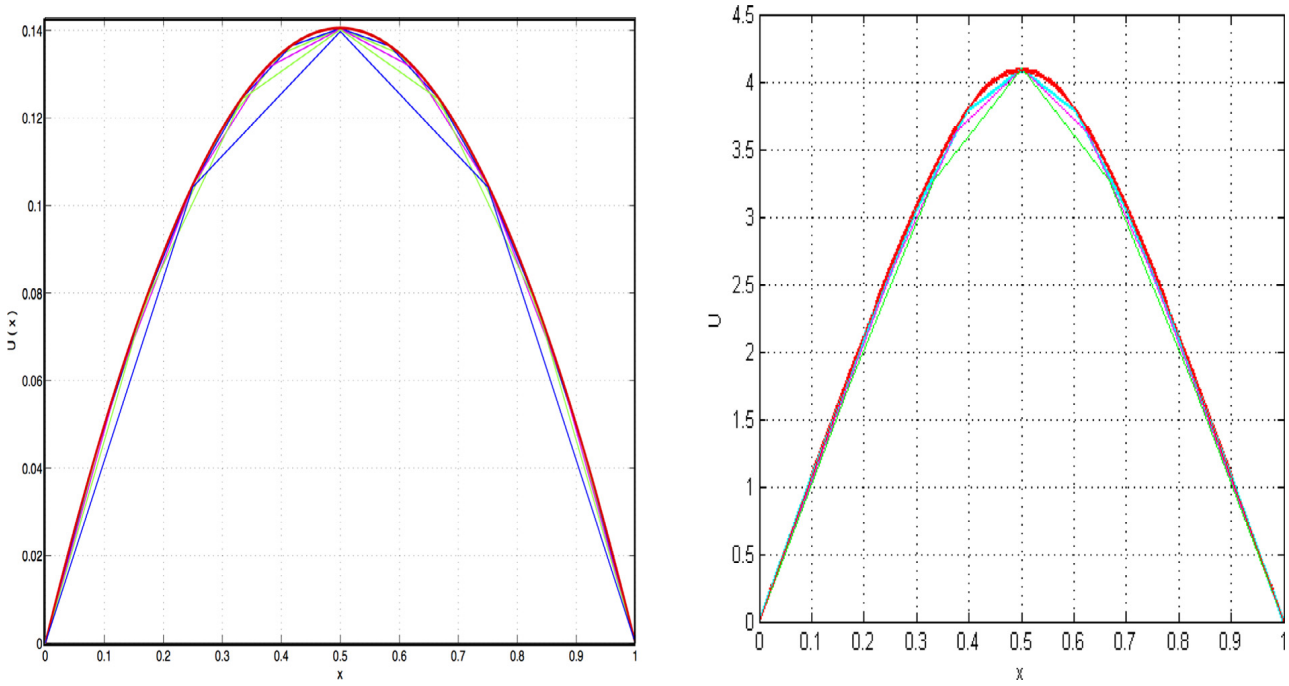

Fig. 6. Numerical convergence behavior of NSFD for $N = \infty$. Comparison of the lower solution (left) and the upper solution (right) by increasing the number of grid points J (for $\lambda = 1$).

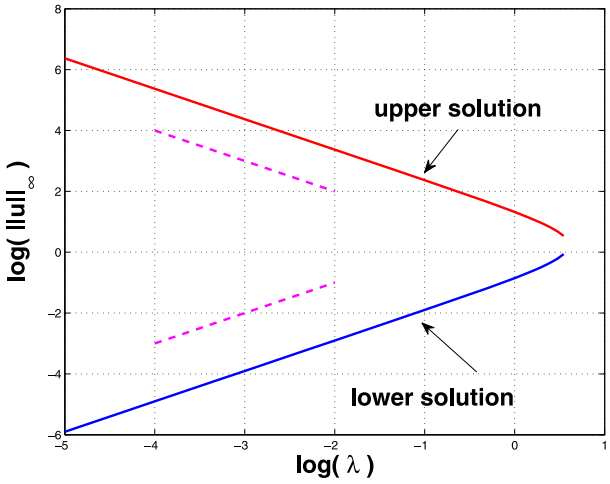

Fig. 7. A $log_{10} - log_{10}$ plot of the maximum value as a function of λ. The dashed lines are straight lines with slope 1 and -1 (see also Table 5) and indicate the asymptotic $\mathcal{O}(\lambda)$ and $\mathcal{O}(\lambda^{-1})$ behaviour of the two solutions for $\lambda \downarrow 0$.

$$u''(x) + \lambda\left(1 + u(x) + \frac{1}{2}u(x)^2 + \frac{1}{6}u(x)^3 + \frac{1}{24}u(x)^4 + \frac{1}{120}u(x)^5\right) = 0. \tag{2.12}$$

These cases also possess the same properties as described for $N \in \mathcal{N}_2 \cup \infty$, when consider the positive solutions (lower, upper and one) only. However, we will show numerically that other solutions exist as well when we discuss both positive and negative solutions. In this situation, the model has *infinitely* many solutions for $\lambda > 0$. These solutions are either periodic or semi-periodic. Of course, numerical calculations are only able to show a (large) finite number of these. A unique solution exists for negative λ values (see Lemma 5). Similar conclusions can be made for the cases $N = 7, 9, \ldots$. Note that the theoretical proof of these observations is given in reference [30].

3. Numerical approximation

In this section, two different finite difference schemes SFD and NSFD are discussed to compute the numerical solutions of the truncated Bratu–Picard problem (1.1). Both schemes are based on the discrete versions of the boundary value problem

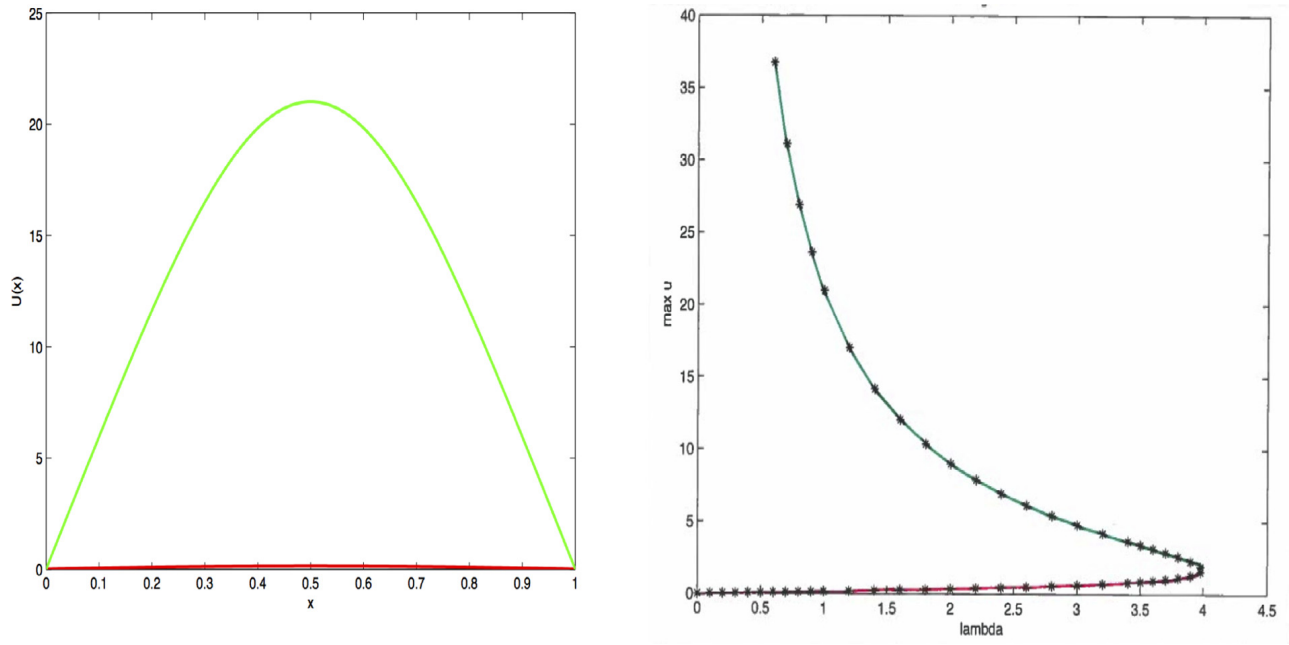

Fig. 8. Lower (red) and upper (green) solution for $N = 2$ and $\lambda = 1$ (left plot). The bifurcation diagram (right plot) shows that this case resembles the $N = \infty$ case. (For interpretation of the references to color in this figure legend, the reader is referred to the web version of this article.)

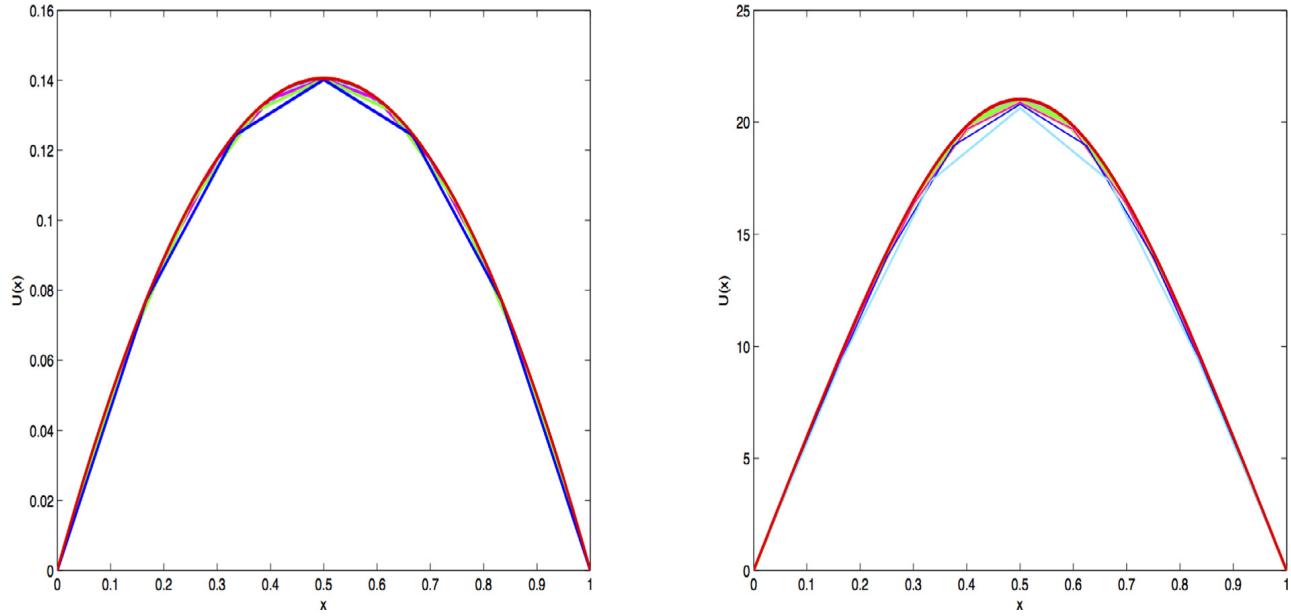

Fig. 9. Numerical convergence of the NSFD method for the two existing solutions for $N = 2$: lower solution (left) and upper solution (right).

by approximating the derivatives and the boundary conditions. To compute the numerical solutions of (1.1) both schemes go with a uniformly distributed spatial grid Δx. These schemes transform problem (1.1) into a system of nonlinear equations which can then be solved by using a suitable iterative method.

3.1. Standard finite differences (SFD)

To compute numerical solutions of the truncated Bratu–Picard model (1.1), we first employ a standard finite difference (SFD) scheme by discretizing the differential equation and boundary conditions. The first step in the computation of the numerical solution of (1.1) is to subdivide the continuous spatial interval $x \in [0, 1]$ with a discrete grid. For this, choose the grid points $\{x_j\}_{j=0}^{J}$ uniformly, i.e., $x_j = j\ \Delta x, \quad j = 0, \ldots, J$ with $\Delta x = \frac{1}{J}$ and approximate the second derivative in (1.1) by the

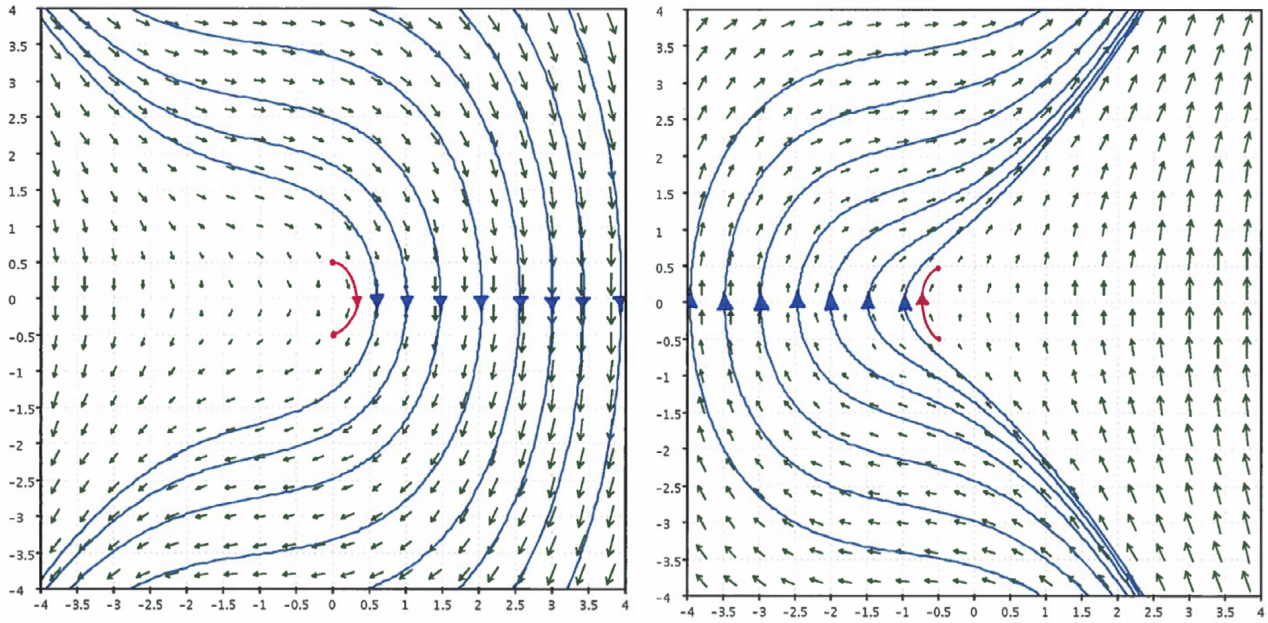

Fig. 10. The phase plane (u, u') for $N = 2$: $\lambda < 0$ (left) and $\lambda > 0$ (right): no critical points are present. Red curves represent solutions satisfying the two boundary conditions. (For interpretation of the references to color in this figure legend, the reader is referred to the web version of this article.)

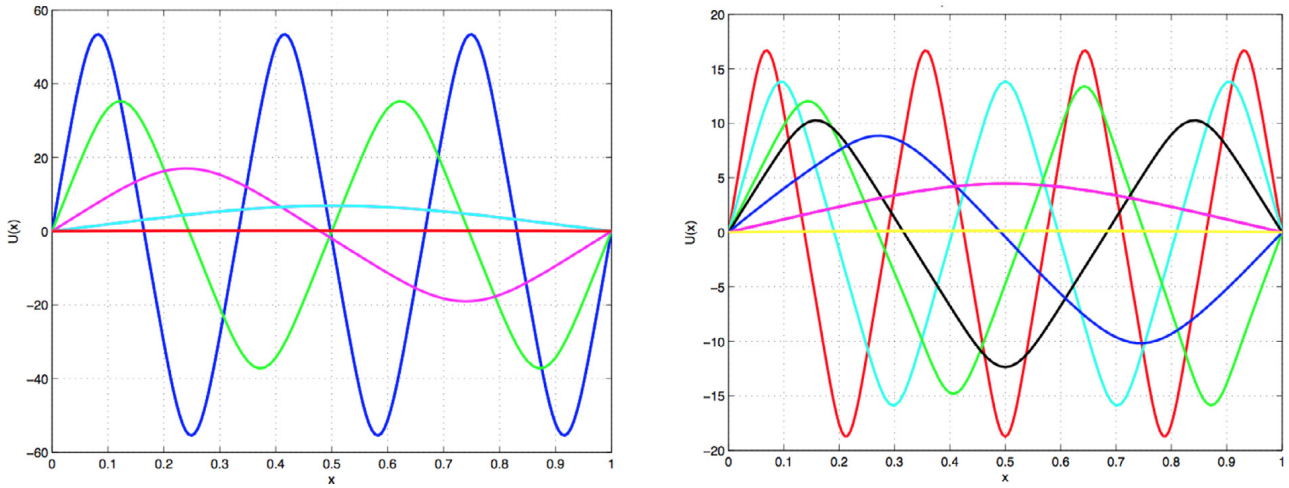

Fig. 11. Five (semi-)periodic solutions for $N = 3$ (left) and seven (semi)-periodic solutions for $N = 5$ (right) with $\lambda = 1$.

second-order approximation:

$$u''(x_j) \approx \frac{u_{j+1} - 2u_j + u_{j-1}}{(\Delta x)^2}, \quad j = 1, \ldots, J-1, \tag{3.1}$$

where $u_j \approx u_\lambda^N(x_j)$. This yields the discrete nonlinear system:

$$\frac{u_{j+1} - 2u_j + u_{j-1}}{(\Delta x)^2} + \lambda \sum_{n=0}^{N} \frac{u_j^n}{n!} = 0, \quad j = 1, \ldots, J-1, \tag{3.2}$$

with $u_0 = u_J = 0$.

3.2. Nonstandard finite differences (NSFD)

A nonstandard finite-difference scheme (NSFD) approximates a derivative by using a denominator function and uses 'non-local' or 'off-grid' representations of expressions in the differential equation [17]. Mickens in [18] showed explicitly that one can find NSFD schemes which produce *exact discrete solutions* of a differential equation. Mickens' discretization of the second

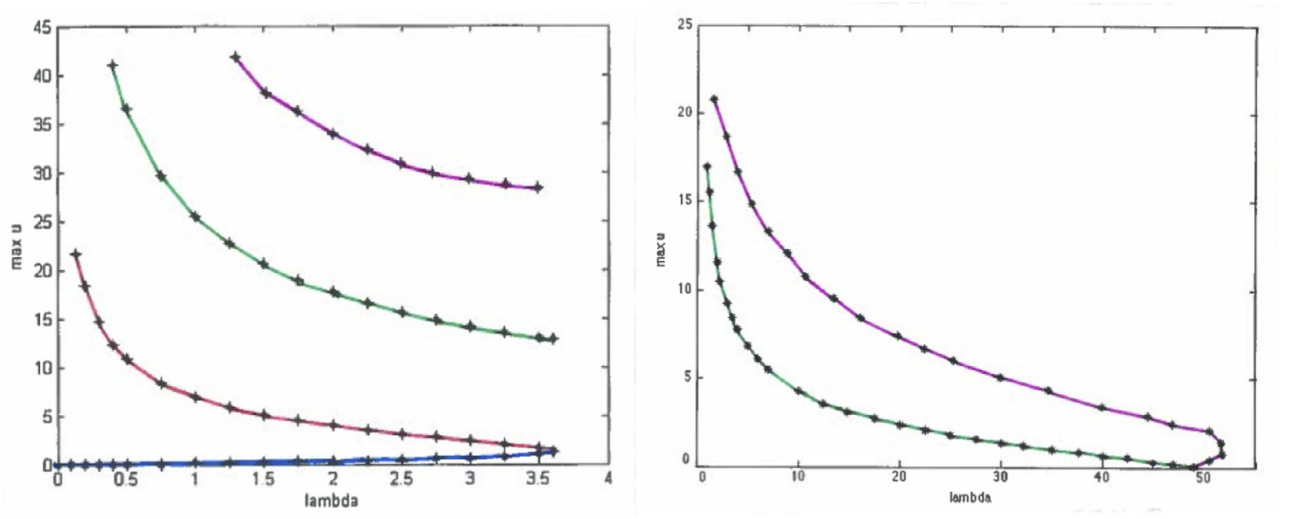

Fig. 12. The numerical bifurcation diagram (left) for $N = 3$ for positive λ. Note that only three curves are displayed. In the right frame numerical approximations of the third (green) and fourth (magenta) solution are shown on an extended λ-interval. These results will be summarized in Fig. 19 and theoretically explained in [30]. (For interpretation of the references to color in this figure legend, the reader is referred to the web version of this article.)

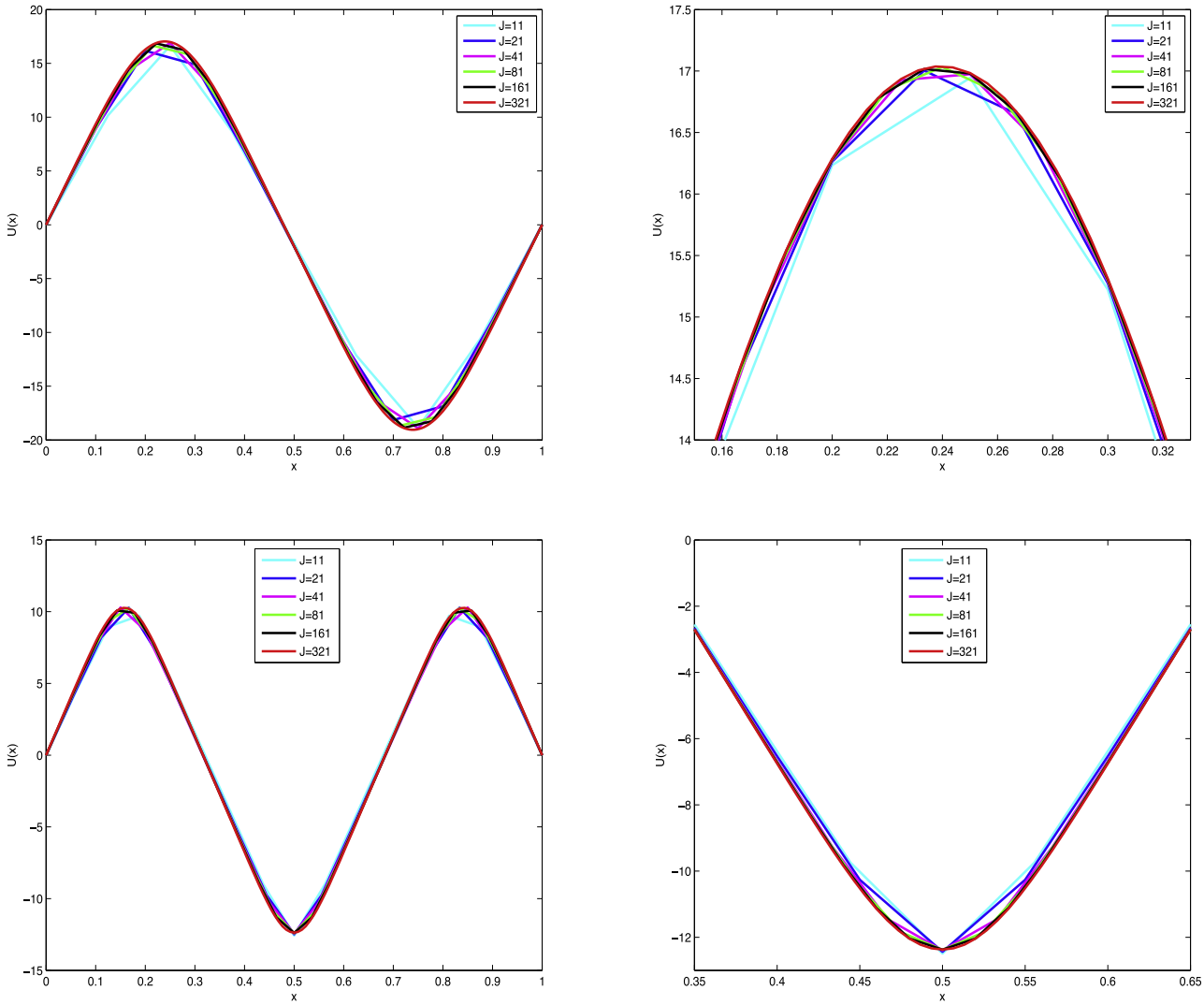

Fig. 13. Convergence of the numerical solution using NSFD for the first periodic solution for $N = 3$ (upper left frame) and a close up near the maximum (upper right frame). Similarly, for the first semi-periodic solution for $N = 5$ (lower left frame) and a close up near the minimum (lower right frame).

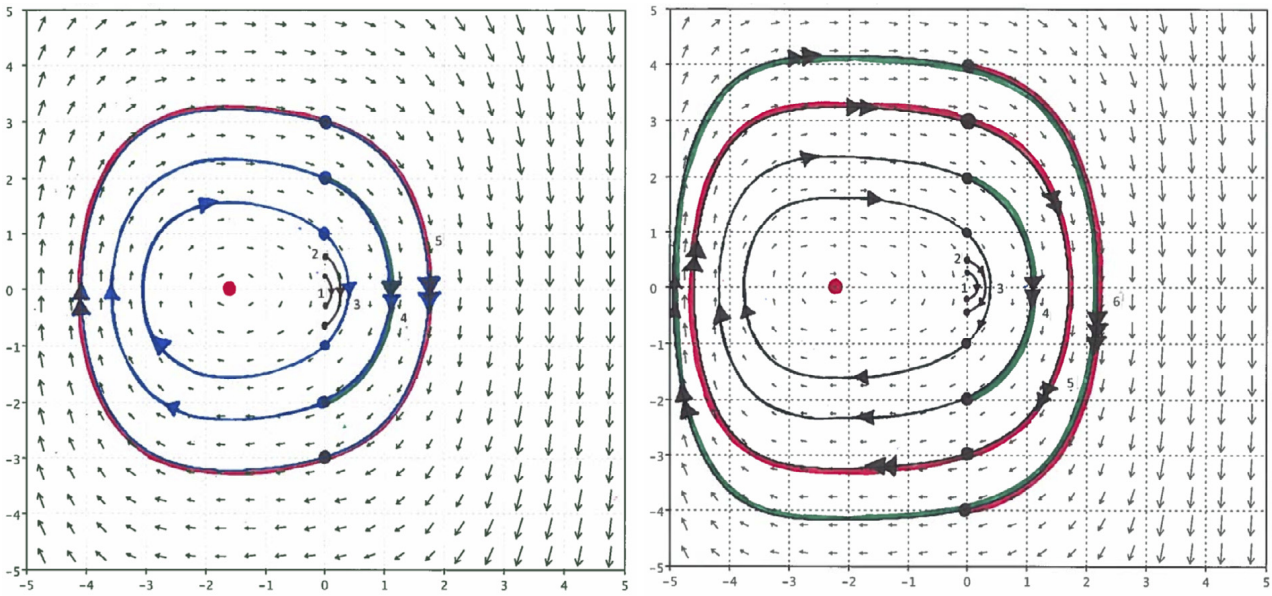

Fig. 14. On the left, the phase plane (u, u') for $N = 3$ and $\lambda = 1$ is displayed. We show five solution curves that satisfy the model and the boundary conditions start from inside to the outside numbered 1 to 5. Initial and final values are indicated by black bullets, the red dot is the critical point of the system. The arrows provide information about the direction and the number of rotations. Solutions 3 and 5 are periodic, solution 4 is semi-periodic and solutions 1 and 2 are similar to the (lower and upper) ones as in the case $N = 2$. On the right we see the phase plane (u, u') for $N = 5$ and $\lambda = 1$. We show six solution curves that satisfy the model and the boundary conditions. Solutions 3 and 5 are periodic, solutions 4 and 6 are semi-periodic and solutions 1 and 2 are similar to the (lower and upper) ones as in the case $N = 2$. We could construct further numerical solutions as well: there is no theoretical, only a numerical, limit. (For interpretation of the references to color in this figure legend, the reader is referred to the web version of this article.)

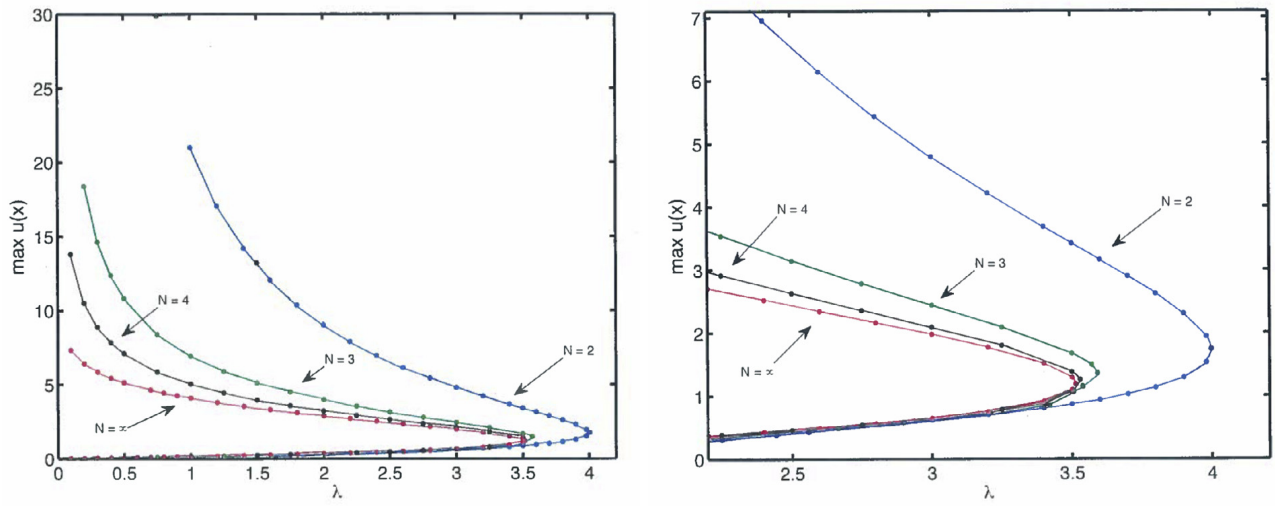

Fig. 15. The numerical convergence of the bifurcation curves (positive solutions for all N) of model (1.1), when N is approaching infinity(left) and a close up near the value $\lambda = \lambda_c$ (right).

derivative has the general form:

$$u''(x_j) \approx \frac{u_{j+1} - 2u_j + u_{j-1}}{\phi(\Delta x)}, \quad j = 1, ..., J-1, \tag{3.3}$$

where the denominator function $\phi(\Delta x)$ has the property

$$\phi(\Delta x) = (\Delta x)^2 + \mathcal{O}((\Delta x)^4) \tag{3.4}$$

Thus, in the limit as $\Delta x \to 0$ the SFD scheme and NSFD scheme will be identical. In [17], the numerical computations are conducted using a nonstandard form of the denominator function $\phi(\Delta x)$ and a 'non-local' discretization of nonlinear terms, that will lead to improving the accuracy for finite values of Δx. A discrete version of a nonstandard finite difference method

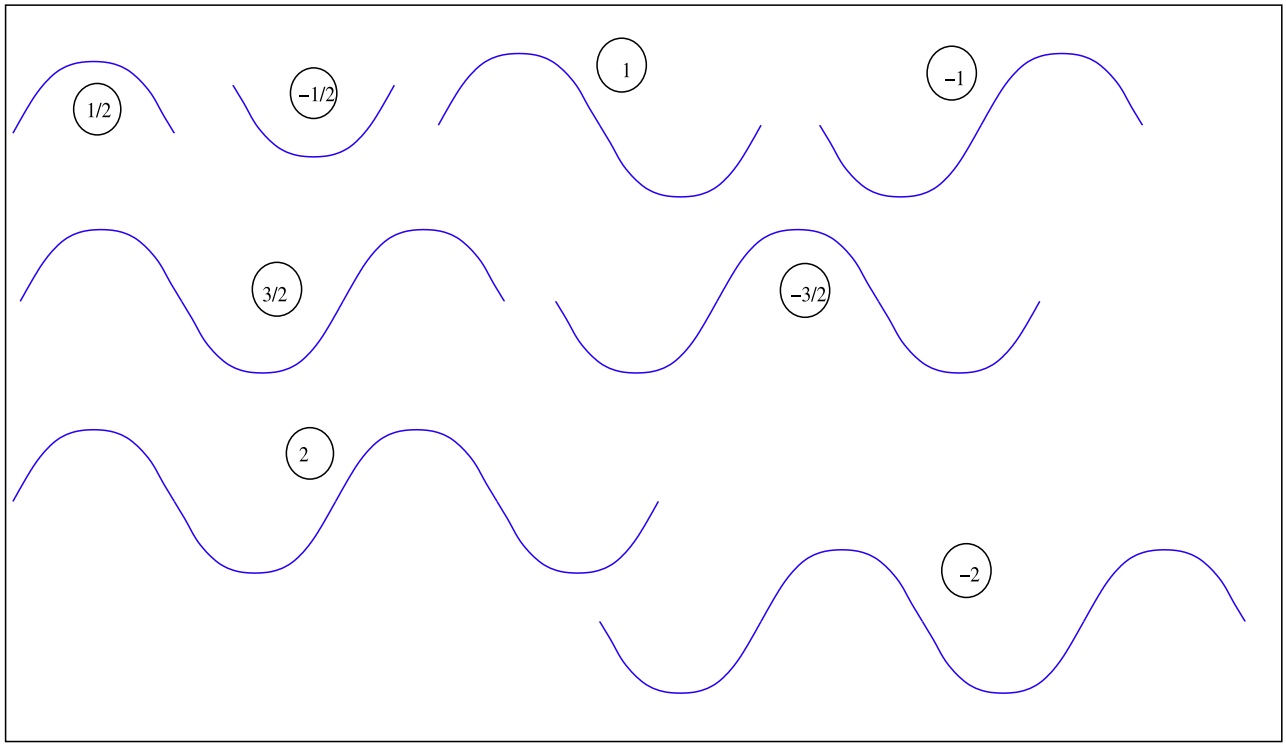

Fig. 16. All possible types of solutions that are shown in Figs. 17–19 can be characterized by a single number. The sign indicates the sign of the slope of the solution at $x = 0$ and the number the periodicity of the solution, respectively. For example, $-3/2$ represents a solution with a first extremum that is negative and has one and a half period which is also denoted as 'semi-periodic' in the main text.

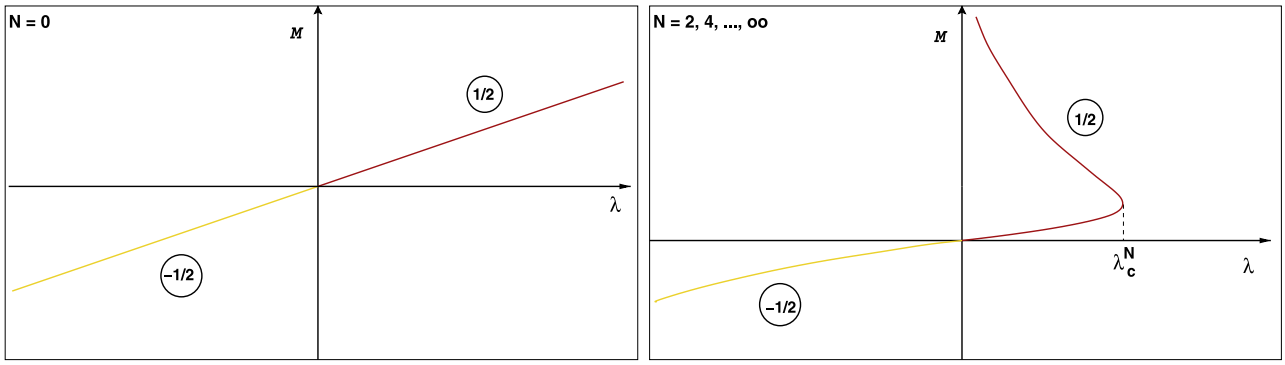

Fig. 17. The analytical bifurcation diagram for $N = 0$ (left) and $N \in \mathcal{N}_2$ (right). The encircled numbers are defined in Fig. 16. The vertical axis is represented by the first extremum M in the solution.

for (1.1) with $\lambda > 0$ is given by

$$\frac{u_{j+1} - 2u_j + u_{j-1}}{2\ln[\cosh(\Delta x)]} + \lambda \sum_{n=0}^{N} \frac{u_j^n}{n!} = 0, \quad j = 1, \ldots, J-1, \tag{3.5}$$

with $u_0 = u_J = 0$ or even replacing the term $\sum_{n=0}^{N} \frac{u_j^n}{n!}$ by a *non-local* version [17]. Note that, e.g., we could use

$$2\ln[\cosh(\Delta x)] = (\Delta x)^2 + \mathcal{O}((\Delta x)^4), \tag{3.6}$$

and

$$2\ln[\cos(\Delta x)] = (\Delta x)^2 + \mathcal{O}((\Delta x)^4). \tag{3.7}$$

These two denominator functions come from the exact solutions (2.8) ($\lambda > 0$) and (2.9) ($\lambda < 0$), respectively. These exact solutions are symmetric and attain their maximum at $x = \frac{1}{2}$. The nonlinear terms involved in the model (1.1) could be approximated in a nonlocal way. For example in (2.10), the nonlinear term u^2 could be discretized not only by u_k^2 or u_{k+1}^2

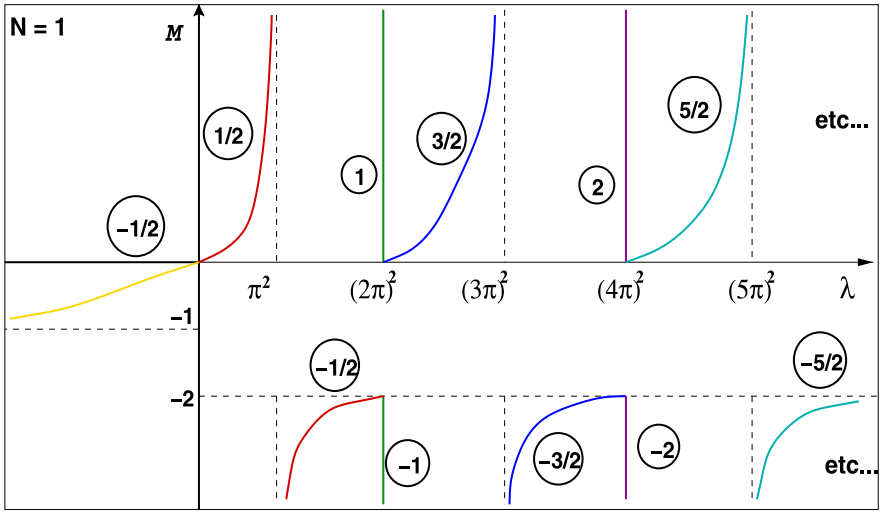

Fig. 18. The analytical bifurcation diagram for $N = 1$. The encircled numbers are defined in Fig. 16. The vertical axis is represented by the first extremum M in the solution.

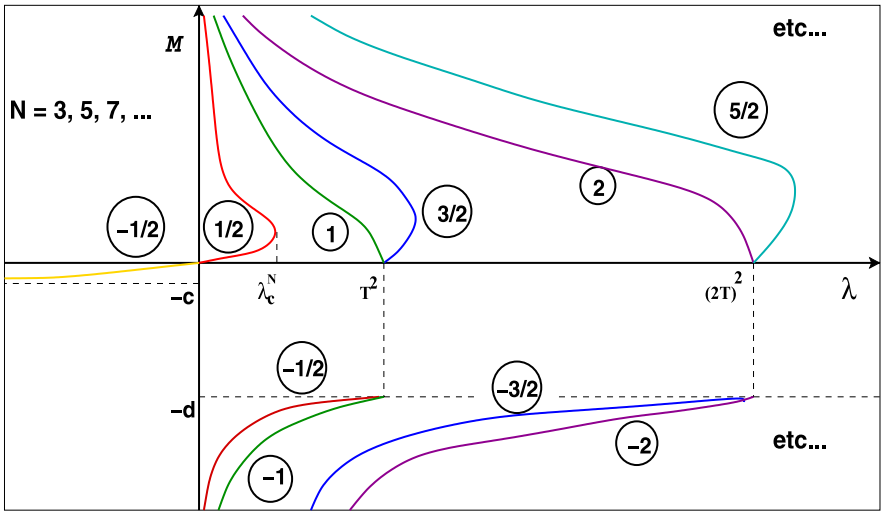

Fig. 19. The analytical bifurcation diagram for $N \in \mathcal{N}_3$. The encircled numbers are defined in Fig. 16. The vertical axis is represented by the first extremum M in the solution.

but by the following:

$$u^2 = \begin{cases} u_k u_{k+1} \\ u_{k-1} u_k \\ u_{k-1} u_{k+1} \\ u_k \left(\dfrac{u_{k+1} + u_k + u_{k-1}}{3} \right) \\ \dots \end{cases} \tag{3.8}$$

In [19], Mickens provides even more types of nonlocal discretizations that may lead to improved accuracy over SFD discretizations. In our computations we did not use the nonlocal discretizations of the nonlinear term in the model, because they only showed minor positive effects.

4. Numerical experiments

To solve the nonlinear systems (3.2) and (3.5), we adopt the simple approach similar to that used by Mohsen [20]. It is appropriate to start the iterations with a sinusoidal function that satisfies the boundary conditions: $u_0(x) = A\sin(k\pi x)$ is the initial guess with an amplitude A and frequency k , to be specified for each case. The values of A and k depend on the index parameters N and λ. In particular, for $\lambda > 0$, to obtain the lower solutions, A should be taken as $A < u_{max}$ and for the upper solutions, we need $A > u_{max}$, where u_{max} is an estimate of the expected maximum value in the solution.

Table 1
lower solution and convergence ratio of the approximation as a function of the number of grid points J for the case with $N = \infty$ and $\lambda = 1$. It shows second order behavior.

J	Standard FDs (3.2)	Ratio	Nonstandard FDs (3.5)	Ratio
5	9.075e−4	6.35	7.433e−4	6.07
11	1.427e−4	4.00	1.223e−4	3.98
21	3.560e−5	4.00	3.071e−5	3.99
41	8.898e−6	3.99	7.683e−6	4.00
81	2.226e−6	3.98	1.919e−6	4.02
161	5.591e−7	3.93	4.773e−7	4.08
321	1.422e−7	3.74	1.168e−7	4.36
641	3.800e−8	–	2.678e−8	–

Table 2
upper solution and convergence ratio of the approximation as a function of the number of grid points J for the case with $N = \infty$ and $\lambda = 1$.

J	standard FDs (3.2)	ratio	nonstandard FDs (3.5)	ratio
5	0.31217	11.15	0.30550	11.64
11	0.02798	4.09	0.02623	4.05
21	0.00684	4.01	0.00647	4.03
41	0.00170	4.00	0.00160	3.99
81	4.251e−4	4.00	4.009e−4	4.00
161	1.062e−4	3.99	1.001e−4	4.01
321	2.656e−5	4.00	2.504e−5	3.99
641	6.639e−6	–	6.260e-6	–

Table 3
Maximum error and convergence ratio of the approximation as a function of the number of grid points J for the case with $N = \infty$ and $\lambda = -1$.

J	standard FDs (3.2)	ratio	nonstandard FDs (3.6)	ratio	nonstandard FDs (3.7)	ratio
5	5.870e−4	6.39	5.428e−4	6.50	5.028e−4	6.16
11	9.175e−5	4.01	8.339e−5	3.97	8.155e−5	3.99
21	2.286e−5	4.00	2.096e−5	3.94	2.042e−5	3.99
41	5.710e−6	4.00	5.312e−6	3.95	5.109e−6	3.99
81	1.427e−6	4.00	1.342e−6	3.99	1.277e−6	3.99
161	3.565e−7	4.01	3.359e−7	3.95	3.197e−7	3.98
321	8.887e−8	4.04	8.492e−8	4.00	8.018e−8	3.99
641	2.197e−8	–	2.118e−8	–	2.009e−8	–

In Fig. 11 which shows solutions for $N = 3$, we take $A = 9$ and $k = 2$ for the first periodic solution. Similarly, for the $N = 5$ case, we take $A = 13$ and $k = 3$ for the first semi-periodic solution. This choice depends on the final number of oscillations that we expect in the solution. The resulting nonlinear system may then be solved iteratively by using an appropriate nonlinear solver. We use Matlab nonlinear routine *fsolve.m*. We tested three cases and computed all numerical solutions with this nonlinear solver. Furthermore, we compare the results obtained from SFD and NSFD schemes and present the bifurcation behaviour of the problem graphically.

4.1. Case 1: $N = \infty$

For this case, the exact solution of the GB-model for positive and negative λ has been discussed in detail in Section 2.4. In this section, we present a numerical comparison between standard and nonstandard finite differences. In the limit $\Delta x \to 0$ both methods coincide. We present the maximum absolute error of SFD and NSFD results by comparing them with the exact solution. We observe that the results show an error which decreases proportionally to $(\Delta x)^2$. The non-standard approximation NSFD only gives more accurate results for moderate values of J.

Tables 1 (lower solution) and 2 (upper solution) show an error comparison between standard and non-standard finite-differences. We observe, as predicted, a second-order convergence, in which the errors in NSFD are slightly smaller than SFD. Furthermore, in Table 3 it is seen that approximation (3.7) yields slightly better results than (3.6) for negative λ-values, as predicted. Note that, NSFD and standard FD are equally accurate in an asymptotic sense $J \to \infty$. Further, we present the numerical solution and convergence of the lower and upper solutions, as [7] reported that NSFD converges both to the lower and the upper solution. Fig. 6 confirms the convergence of both solutions (lower and upper).

Table 4
Maximum error for the *lower* solution, as a function of the number of grid points J for the case with $N = 2$ and $\lambda = 1$: a comparison between three FD schemes.

J	SFD	NSFD1	NSFD2
5	9.032e−3	4.2993e−3	7.454e−4
11	2.421e−3	9.482e−4	1.227e−4
21	7.543e−4	2.681e−4	3.080e−5
41	8.842e−5	4.198e−5	7.719e−6
81	2.199e−5	1.048e−5	1.941e−6
161	5.423e−6	2.609e−6	4.853e−7
321	6.357e−7	1.418e−7	3.186e−8

Table 5
Maximum values for the lower and upper solution in the case $N = 2$. It confirms the asymptotic analysis in Lemma 7 (see also Fig. 7).

λ	$\|\|u\|\|_\infty^{lower}$	$\|\|u\|\|_\infty^{upper}$
0.1	0.01263	2.335e+2
0.01	0.00125	2.356e+3
0.001	1.250e−4	2.358e+4
0.0001	1.250e−5	2.358e+5
0.00001	1.249e−6	2.358e+6

4.2. Case 2: $N \in \mathcal{N}_2$

To investigate this case, we take example (2.10) as discussed in Section 2.5. We adopt two NSFD schemes to obtain numerical results. In NSFD1, the denominator function comes from Mickens' exact finite difference scheme [18], whereas in NSFD2 the denominator function is as derived from the exact solution already mentioned in [7] and [20]. We use the following abbreviations:

$$NSFD1: \ u''(x)|_{x_j} \approx \frac{u_{j+1} - 2u_j + u_{j-1}}{\frac{4}{\lambda}\sin^2\left(\frac{\sqrt{\lambda}\Delta x}{2}\right)} \tag{4.1}$$

(a non-standard FD method, as described in [18],

$$NSFD2: \ u''(x)|_{x_j} \approx \frac{u_{j+1} - 2u_j + u_{j-1}}{2\ln(\cosh(\Delta x))} \tag{4.2}$$

(non-standard FDs, as described in [7] and [20]).

Table 4 gives the comparison of three FD approximations for the lower solution and $\lambda = 1$. It is observed that the NSFD schemes are slightly more accurate than the SFD scheme and that the proposed denominator function in NSFD2 performs better than the originally derived one from [18].

Further, to support the result of Lemma 7, we perform a series of numerical tests for decreasing values of λ (see Table 5 and Fig. 7). We find the expected behavior as predicted by Lemma 7: for the lower solution $||u_\lambda||_\infty = \mathcal{O}(\lambda)$ and for the upper solution $||u_\lambda||_\infty = \mathcal{O}(\frac{1}{\lambda})$. Fig. 8 shows the upper and lower solution for $\lambda = 1$ (left panel) and the bifurcation curve for positive λ in this situation (right panel). It is similar to the case $N = \infty$, but now with $\lambda_c \approx 3.96$. Furthermore, Fig. 9 shows the numerical convergence of both solutions (lower and upper) for this case. The phase plane (u, u'), for the $N = 2$ case, is given in Fig. 10. No critical points are present. The solutions satisfying the boundary conditions are represented by the red curves.

4.3. Case 3: $N \in \mathcal{N}_3$

In this case we discuss the two examples (2.11) and (2.12) as mentioned in Section 2.6. These examples illustrate the fact that we expect infinitely many solutions for this case. These solutions may be periodic or semi-periodic. We again adopt the three FD schemes for comparing the numerical solutions. We consider the first semi-periodic solution for $N = 3$ and $\lambda = 1$ in the numerical comparison which is shown in Table 6. This comparison illustrates that NSFD1 is more accurate than other two FD approximations whereas NSFD2 is slightly better than SFD. Fig. 11 displays five (semi)-periodic solutions for $N = 3$ and seven (semi)-periodic solutions for $N = 5$, respectively. To characterize the bifurcation nature, we consider the relative maximum solution (consider the positive solutions) only. Fig. 12 shows the bifurcation curve for positive λ in which lower, upper and (semi)-periodic solution curves are displayed for this situation. Fig. 13 confirms that the NSFD method converges to the solutions (periodic and semi-periodic) for $N \in \mathcal{N}_3$. Phase plane plots for this case are given in Fig. 14, which shows the different types of solutions: periodic and semi-periodic.

Table 6
Maximum error for the 'first' semi-periodic solution as a function of the number of grid points J for the case with $N = 3$ and $\lambda = 1$: a comparison between three FD schemes.

J	SFD	NSFD1	NSFD2
11	0.90648	0.07832	0.39244
21	0.09455	0.00964	0.06074
41	0.06531	0.00120	0.01436
81	0.00836	1.762e−4	0.00399
161	9.811e−4	8.923e−5	3.321e−4
321	2.099e−4	2.950e−5	7.801e−5

Table 7
The dependence of the critical value λ_c on the index N in the model and its accuracy as a function of the number of grid points J.

N	0	1	2	3	5	10	50	...	∞
$J = 21$	–	–	3.9970	3.6211	3.5712	3.5621	3.5283	...	3.51387
$J = 41$	–	–	3.9613	3.6000	3.5649	3.5561	3.5234	...	3.51384
$J = 81$	–	–	3.9600	3.5991	3.5612	3.5511	3.5224	...	3.51384

Remark

Model (1.1) is actually the classical Gelfand–Bratu problem when N is approaching infinity. We discussed the behavior of the solutions of model (1.1) and other cases, which depend on the index N. For all N, we obtained a bifurcation curve for positive solutions (lower, upper and one solution). When we allow periodic and semi-periodic solutions (with possible negative values) then we obtained extra curves, as mentioned in Section 4.3. Fig. 15 shows the numerical convergence (N approaching infinity) of the bifurcation curves (positive solutions only) for all N of model (1.1). When we take the limit N approaching infinity, the bifurcation curves move towards the curve for $N = \infty$. This limit can be both uniform and non-uniform. For positive solutions, the limit is uniform for all N and non-uniform for the case $N = 3, 5, 7, \ldots$ (with periodic and semi-periodic solutions).

5. Epilogue

In this final section we summarize all our theoretical and numerical results. Figs. 16–19 display all types of solutions and bifurcations connected with model (1.1). In Fig. 16 we show the possible shapes of the periodic and semi-periodic solutions. The encircled numbers indicate the period for each case and the sign whether the first extremum in the solution is a maximum (+) or a minimum (−), respectively. Figs. 17–19 illustrate the relation between the first extremum M and the parameter λ in model (1.1). Note that, in Fig. 19 (the case $N \in \mathcal{N}_3$) the parameters c, d and T are defined in the following way. The value of $-c$ corresponds with the location of the center point in the phase plane (see also the red dot in Fig. 14) and the value of $-d$ is the intersection of the periodic orbit going through $(u, u') = (0, 0)$ with the u-axis. The period of this orbit is denoted by T. We observe that, for $N = 1$, we obtain $c = 1$, $d = 2$ and $T = 2\pi$, as can be seen in Fig. 18. It is also interesting to mention that the curves in Fig. 19 ($N \in \mathcal{N}_3$) are deformations of the ones in Fig. 18 ($N = 1$). This behavior will be theoretically explained in an upcoming paper [30].

6. Summary

In this paper, we presented numerical solutions of a truncated Bratu–Picard model by using both standard and nonstandard finite difference approximations. Solutions $u_\lambda^N(x)$ depending on the parameter λ and N were constructed by applying the nonlinear solver routine fsolve.m of Matlab. We described a series of theoretical properties of the solutions of model (1.1). For example, we analyzed the symmetry, the asymptotic behaviour and the uniqueness of the solutions for all indices N and all values of the parameter λ. For the complete numerical interpretation of model (1.1) we distinguish the problem in different cases. By using the FD approximations, numerical results showed the existence of two, one and zero solutions for $\lambda > 0$ and $N \in \mathcal{N}_2$, which resembles the $N = \infty$ case.

Investigation of the case $N \in \mathcal{N}_3$ indicated, that we obtain infinitely many solutions, which are calculated numerically (for a large, but finite, set of solutions). These solutions are either periodic or semi-periodic which can be explained in phase plane (u, u') diagrams. We also presented the bifurcation nature of model (1.1) for each case. We compared several finite difference schemes and we observed that with an appropriate initial guess having a suitable amplitude, the NSFD schemes provide more accurate results than the SFD scheme. We also found numerically that the NSFD approximations converge to the solutions (the lower and upper one) for each case. Further, Tables 7 and 8 summarize results on the location of the critical value λ_c and on the type of solution, depending on N and λ, respectively. In these graphs, the vertical axis is represented by the number M, which denotes the value of the first extremum that appears in the solution, counted from the

Table 8
The dependence of the number of solutions on the index N and λ. For $N = 0$ there is a unique solution of (1.1), for $N = 1$ we have a unique solution for $\lambda \in \mathbb{R}$ (except for $\lambda = 4\pi^2, 9\pi^2, \ldots$ for which there are infinitely many solutions), for $N \in \mathcal{N}_2$ the number of solutions of Eq. (1.1) can be zero (for $\lambda > \lambda_c$), one (for $\lambda \leq 0$ and for $\lambda = \lambda_c$) or two (for $0 < \lambda < \lambda_c$) and for $N \in \mathcal{N}_3$ only a unique solution exists for $\lambda \leq 0$, respectively. In the latter case, we obtain infinitely many solutions of (1.1) for $\lambda > 0$.

N	0	1	2	3	4	5	6	7	...	∞
# solutions	1	1, ∞	0, 1, 2	1, ∞	0, 1, 2	1, ∞	0, 1, 2	1, ∞	...	0, 1, 2

left boundary. Finally, in the upcoming paper [30] the authors report on all theoretical aspects connected with the results depicted in Fig. 19.

Acknowledgments

Sehar Iqbal acknowledges the financial support by the Schlumberger Foundation (Faculty for the Future). The authors would like to thank André Zegeling and Ferdinand Verhulst for interesting discussions and for their valuable comments.

References

[1] S. Abbasbandy, M.S. Hashemi, C. Liu, The Lie-group shooting method for solving the Bratu equation, Numer. Simul. 16 (2011) 4238–4249.
[2] R.P. Agarwal, D. O'Regan, R.J.Y Wong, Positive Solutions of Differential, Difference and Integral Equations, Kluwer Academic Publishers, 1999.
[3] T. Bakri, Y. Kuznetsov, F. Verhulst, E. Doedel, Multiple solutions of a generalized singular perturbed Bratu problem, Int. J. Bifurc. Chaos 22 (4) (2012).
[4] J. Bebernes, D. Eberly, Mathematical problems from combustion theory, Applied Mathematics Science, vol. 83, Springer, 1989.
[5] G. Bratu, Sur les equations integrals non lineaires, Bulletin de la S.M.F. 42 (1914) 113–142.
[6] M. Bratu, Sur l'equation integrale exponentielle, Comptes Rendus des Seances de l'academie des sciences (1911) 1048–1050.
[7] R. Buckmire, Application of a Mickens finite-difference schem to the cylindrical Bratu-Gelfand problem, Numer. Methods Partial Differ. Equ. 20 (3) (2004) 327–337.
[8] S. Chandrasekhar, An Introduction to the Study of Stellar Structure, Dover, 1967.
[9] W. Eckhaus, Matched asymptotic expansions and singular perturbations, Mathematics Studies, 6, North-Holland, 1973.
[10] U. Erdogan, T. Ozis, A smart nonstandard finite difference scheme for second order nonlinear boundary value problems, J. Comput. Phys. 230 (2011) 6464–6574.
[11] I. Gelfand, Some problems in the theory of quasi-linear equations, Amer. Math. Soc. Transl. Ser. 2 (29) (1963) 295–381.
[12] S. Hastings, J. McLeod, Classical methods in ordinary differential equations: with applications to boundary value problems, Graduate Studies in Mathematics, 129, American Mathematics Society, 2011.
[13] H. Temimi, M. Ben-Romdhane, An iterative finite difference method for solving Bratu's problem, J. Comput. Appl. Math. 292 (2016) 76–82.
[14] J.P. Boyd, One-point pseudospectral collocation for the one dimensional Bratu equation., Appl. Math. Comput. 217 (2011) 5553–5565.
[15] P. Korman, Y. Li, T. Ouyang, Exact multiplicity results for boundary value problems with nonlinearities generalizing cubic, Proc. R. Soc. Edinburgh 126 (3) (1996) 599–616.
[16] T. Laetsch, The number of solutions of a nonlinear two point boundary value problem, Indiana Univ. Math. J. 20 (1) (1970).
[17] R. Mickens, Difference equation models of differential equations having zero local truncation error, vol. 92 of North-Holland Mathematics Studies, Elsevier Science Publishers B.V., pp. 445–449.
[18] R. Mickens, Nonstandard finite difference models of differential equations, World Sci., 1993.
[19] R. Mickens, A best finite-difference scheme for the Fisher equation, Numer. Meth. Partial Differ. Equ. 10 (1994) 581–585.
[20] A. Mohsen, A simple solution of the Bratu problem, Comput. Math. Appl. 67 (2014) 26–33.
[21] A. Mohsen, L. Sedeck, S. Mohamed, New smoother to enhanced multigrid-based methods for the Bratu problem, Appl. Math. Comput. 204 (2008) 325–339.
[22] A. Mounim, B. de Dormale, From the fitting technique to accurate schemes for the Liouville-Bratu-Gelfand problem, Numer. Meth. Partial Differ. Equ. 22 (2006) 761–775.
[23] E. Picard, Sur certains exemples singuliers d'approximations successives, Comptes Rendus des Seances de l'academie des sciences (1898) 497–500.
[24] A. Polyanin, V. Zaitsev, Handbook of Exact Solutions for Ordinary Differential Equations, CRC Press, Inc., 1995.
[25] R.E. O'Malley Jr, Phase-plane solutions to some singular perturbation problems, J. Math. Anal. Appl. 54 (1976) 449–466.
[26] I. Shufrin, O. Rabinovitch, M. Eisenberger, Elastic nonlinear stability analysis of thin rectangular plates through a semi-analytical approach, Int. J. Solids Struct. 46 (2009) 2075–2092.
[27] F. Verhulst, Methods and Applications of Singular Perturbations, Springer, 2005.
[28] Y. Wan, Q. Guo, N. Pan, Thermo-electro-hydrodynamic model for electrospinning process, Int. J. Nonlinear Sci. Numer. Simul. 5 (1) (2004) 5–8.
[29] A. Wazwaz, Adomian's decomposition method for a reliable treatment of the Bratu-type equations, Appl. Math. Comput. 166 (2005) 652–663.
[30] A. Zegeling, P.Zegeling, Bifurcations of solutions to nonlinear ODE boundary value problems, 2018, In preparation.